Diffusion of Particles in the Extracellular Matrix: The Effect of Repulsive Electrostatic Interactions

Triantafyllos Stylianopoulos,[†] Ming-Zher Poh,[†] Numpon Insin,[‡] Moungi G. Bawendi,[‡] Dai Fukumura,[†] Lance L. Munn,[†*] and Rakesh K. Jain[†*]

[†]Edwin L. Steele Laboratory, Department of Radiation Oncology, Massachusetts General Hospital and Harvard Medical School, Boston, Massachusetts; and [‡]Department of Chemistry, Massachusetts Institute of Technology, Cambridge, Massachusetts

ABSTRACT Diffusive transport of macromolecules and nanoparticles in charged fibrous media is of interest in many biological applications, including drug delivery and separation processes. Experimental findings have shown that diffusion can be significantly hindered by electrostatic interactions between the diffusing particle and charged components of the extracellular matrix. The implications, however, have not been analyzed rigorously. Here, we present a mathematical framework to study the effect of charge on the diffusive transport of macromolecules and nanoparticles in the extracellular matrix of biological tissues. The model takes into account steric, hydrodynamic, and electrostatic interactions. We show that when the fiber size is comparable to the Debye length, electrostatic forces between the fibers and the particles result in slowed diffusion. However, as the fiber diameter increases the repulsive forces become less important. Our results explain the experimental observations that neutral particles diffuse faster than charged particles. Taken together, we conclude that optimal particles for delivery to tumors should be initially cationic to target the tumor vessels and then change to neutral charge after exiting the blood vessels.

INTRODUCTION

Diffusion of macromolecules and nanoparticles in the extracellular matrix (ECM) is crucial for the delivery of therapeutic agents in tumor tissues (1). Recent advances in nanotechnology have led to the development of particles with controllable size and surface charge and with the potential to be used for cancer detection and treatment (2,3). Now there is an emerging need for a better understanding of how these particles diffuse in the ECM and for prediction of the particle properties that optimize their delivery to cancer cells.

The movement of particles in tissues depends on their size, charge, and configuration as well as the physicochemical properties of the ECM (1). The ECM is mainly composed of a network of collagen fibers and other molecules such as hyaluronic acid. Particles perform Brownian random walks through the spaces between network structures and are influenced by components of the matrix in three distinct ways: i), they collide with matrix fibers (steric interactions), ii), as they diffuse near fibers, restricted thermal motion of water molecules due to proximity to the fibers slows their diffusion (hydrodynamic interactions), and iii), for charged particles, electrostatic interactions with charged components of the extracellular matrix contribute an additional force.

The effect of steric and hydrodynamic interactions on the diffusion of nanoparticles in fibrous media has been studied extensively both experimentally (4–9) and with the use of mathematical modeling (10–16). On the other hand, little is known about the effects of electrostatic forces on diffusion. Experimental work has been focused on the effect of electrostatic attraction between charged particles and components of the ECM of opposite charge and particularly with heparan sulfate (17–20). These studies have shown that particles bind to the surface of the extracellular fibers, which can decrease their effective diffusivity by three orders of magnitude. Electrostatic repulsion, however, as well as the effect of parameters such as fiber volume fraction and fiber and particle diameter on electrostatic forces have not been studied as thoroughly as electrostatic attraction. Given the fact that the charge of therapeutic drugs and nanoparticles can vary from highly negative to neutral to highly positive, we developed a comprehensive theoretical framework that takes into account electrostatic repulsion, as well as steric and hydrodynamic interactions.

To model the interstitial space, we used a three-dimensional spatially periodic square array of fibers (Fig. 1). We employed i), a random walk approach (11,15) to simulate the diffusion of nanoparticles, ii), Stokesian dynamics (12) to account for hydrodynamic hindrance, and iii), a correlation developed by Johnson and Deen (21) to calculate electrostatic energies between the fibers and the diffusing particle. We first validated our approach with a published model (12) that accounts for only steric and hydrodynamic hindrances as well as with our experimental data for the diffusivity of semiconductor nanocrystals (quantum dots) in collagen gels. Then, we employed the model to study how electrostatic interactions affect the diffusivity of particles. Finally, we used our model predictions and published studies (17,18) to offer guidelines for the optimal design of nanoparticles for drug delivery to tumors.

Submitted February 22, 2010, and accepted for publication June 9, 2010.

*Correspondence: jain@steele.mgh.harvard.edu or lance@steele.mgh.harvard.edu

Editor: Nathan Andrew Baker.

0006-3495/10/09/1342/8 $2.00

doi: 10.1016/j.bpj.2010.06.016

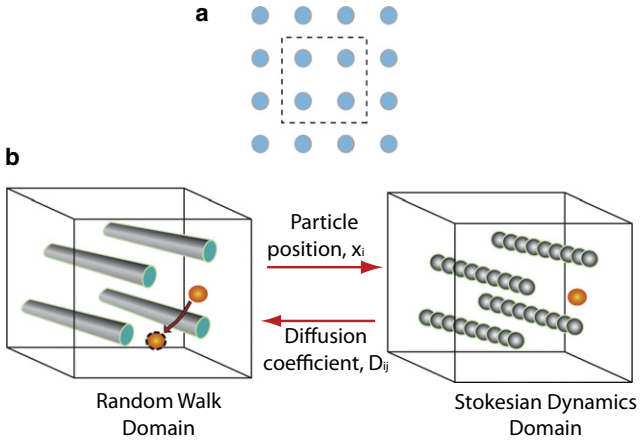

FIGURE 1 (*a*) Collagen fibers are represented as a spatially periodic square array of fibers and our analysis is performed in a periodic unit cell shown by the dashed line. (*b*) Nanoparticles diffuse inside the fibrous medium (random walk domain). A second computational domain is constructed for the calculation of hydrodynamic interactions (Stokesian dynamics domain). At each time step of the random walk, the position of the particle is mapped to the Stokesian dynamics domain and its diffusion coefficient is calculated by the solution of a Stokesian dynamics problem. The diffusion coefficient is returned to the random walk domain and the nanoparticle is moving to a new randomly chosen position. The new position is accepted with a probability $\exp(-\Delta E/kT)$, where ΔE is the electrostatic energy difference between the two positions, k is the Boltzmann's constant and T is the temperature. Periodic boundary conditions are applied and in case of collision with a fiber the displacement is rejected.

METHODS

Model formulation

The computational domain consisted of a three-dimensional, spatially-periodic, square array of fibers and the analysis was performed in a periodic unit cell (Fig. 1 *a*). Particles were randomly distributed inside the domain, where they performed a random walk. According to the random walk method, the diffusing particle moved stepwise inside the fiber medium along a randomly chosen direction. At each elementary time step, Δt, the displacement, δ, of the particle in each coordinate direction, i, was determined by $\delta_i = \sqrt{2D_{ii}\Delta t}$, where D_{ij} is the local diffusion coefficient tensor.

Diffusion of the particle is hindered due to hydrodynamic interactions and is determined by Stokesian dynamics. For the Stokesian dynamics approach, a second computational domain was constructed where the fibers were represented as lines of adjacent spheres (bead and string model (12,22)) with the same diameter as that of the fibers. At each time step the position of the particle, x_i, was mapped from the random walk domain to the Stokesian dynamics domain, the Stokesian dynamics problem was solved, and the local diffusion coefficient tensor of the particle, D_{ij}, was determined based on the size of the particle and its position inside the network (Fig. 1 *b*). The local diffusion coefficient decreases as the particle size increases or as the particle approaches the fibers. Finally, the local diffusion coefficient was returned to the random walk domain and the particle was displaced to its new randomly chosen position.

Next, we checked if the displacement resulted in collision with the fibers or crossing the boundary of the random walk domain. In the first case, the displacement was rejected and the position of the particle did not change, whereas in the second case periodic boundary conditions were applied (11,15). To account for electrostatic interactions, the particle was allowed to move to positions of lower energy or to positions of higher energy with a probability of $\exp(-\Delta E/kT)$, where ΔE is the electrostatic energy difference between the new and the previous position, k is the Boltzmann's constant, and T is the temperature. Therefore, if the particle did not collide with any of the fibers, the difference in the electrostatic energy between the new and the previous position, ΔE, was calculated. A random number was then generated and if $\exp(-\Delta E/kT)$ was higher than this random number, the new position was accepted.

By tracking the trajectory of the particle for 10,000 time steps and taking the average over 1000 particles, the overall diffusion coefficient, D, as well as the components of the main diagonal of the overall diffusion coefficient tensor $(D^*_{xx}, D^*_{yy}, D^*_{zz})$ were determined as

$$D = \frac{< MSD >}{6t}, D^*_{xx} = \frac{< MSD_x >}{2t}, \quad D^*_{yy} = \frac{< MSD_y >}{2t}, \text{ and } D^*_{zz} = \frac{< MSD_z >}{2t}, \tag{1}$$

where t is the time, and the mean-square displacements were calculated from

$$< MSD > = \frac{1}{n}\sum_{i=1}^{n}\left[(x_i(t) - x_i(0))^2 + (y_i(t) - y_i(0))^2 + (z_i(t) - z_i(0))^2\right] \tag{2}$$

$$< MSD_x > = \frac{1}{n}\sum_{i=1}^{n}(x_i(t) - x_i(0))^2,$$

$$< MSD_y > = \frac{1}{n}\sum_{i=1}^{n}(y_i(t) - y_i(0))^2,$$

$$< MSD_z > = \frac{1}{n}\sum_{i=1}^{n}(z_i(t) - z_i(0))^2,$$

where n is the total number of walkers (a thousand in our case) and x_i, y_i, z_i are the coordinate directions of the walker, i.

For the results presented in this study, we plot the overall diffusion coefficient transverse to the preferred fiber direction, $D_\perp$. The fibers are oriented in the z-direction, and thus $D_\perp$ is the average of D^*_{xx} and D^*_{yy}, $D^*_{xx} \approx D^*_{yy}$. Results for the overall diffusivity in the preferred fiber direction, i.e., $D_{||} = D^*_{zz}$,are shown in the Supporting Material.

To calculate the deviations in the solution of our mathematical model due to its stochastic nature, we repeated the simulations and found a $< 3\%$ variation. Incorporation of hydrodynamic forces increased the computational cost dramatically. To make the computations feasible we employed parallel processing and the solution time using 28 processors was ~1 h.

Hydrodynamic interactions

To calculate the hydrodynamic hindrance, we followed the Stokesian dynamics methodology as described in Phillips et al. (12). In a stagnant fluid and ignoring interactions between the diffusing particles, the force, F_i, and the velocity, U_i, of each of the particles is given by the equation

$$F_i = R_{ii}U_i, \tag{3}$$

where R_{ii} is the resistance matrix of the particle. For free diffusion in a solution, the diagonal components of the resistant matrix are equal to each other and are given from the well known Stokes-Einstein relationship as $6\pi\mu r_s$, where μ is the fluid viscosity, and r_s the radius of the particle.

In a fibrous medium, the resistance matrix is determined by separating short-range and long-range hydrodynamic interactions between the particle

and the fibers. To calculate the resistance matrix we represented the fibers as lines of adjacent spheres and used theories developed for sphere-sphere interactions. For the long-range interactions, we employed the Ewald sum of the Rotne-Pranger tensor (23) accounting only for the translational velocity of the particles. This method includes the far-field interactions among all spheres. The resistance matrix still lacks, however, short-range interactions. To incorporate short-range (lubrication) forces, we calculated the interaction between the particle and each of the spheres separately using the exact two-sphere results from the literature (24,25). Therefore, lubrication interactions are calculated in a pair-wise additive fashion under the assumption that the other spheres in the periodic unit cell are negligible. This approach of including lubrication has been tested previously for ordered and disordered arrays of spheres and has been found to agree well with published theoretical and experimental studies (12,26–28). Addition of the long-range and short-range interactions gives the complete approximation to the resistance matrix, R_{ij}. Finally, by applying the generalized form of the Stokes-Einstein relationship, the diffusion coefficient matrix is determined as

$$D_{ii} = kT(R_{ii})^{-1}, \quad (4)$$

where k is the Boltzmann's constant and T is the absolute temperature. The number of spheres that comprised each fiber was determined by repeating test simulations and increasing the number of the spheres. We found that the results were not changed by $>$ 2–3% when more than eight spheres per fiber were used.

Electrostatic interactions

There are not many published studies to calculate the electrostatic energy of a diffusing particle in a fibrous medium and these studies are limited only to interactions between a particle and a single fiber (21,29,30). Recently, the methodology developed by Johnson and Deen (21) was used for a spatial periodic array of fibers (31) and it was found that the total electrostatic energy is calculated in good accuracy by simply adding up the individual contribution of each fiber. According to this methodology, the electrostatic energy between a spherical particle and a fiber scales as

$$E = \frac{(RT/F)^2 \varepsilon r_s}{kT} \Delta G, \quad (5)$$

where R is the gas constant, T is the absolute temperature, ε is the permittivity, r_s is the radius of the particle, k is the Boltzmann's constant, and ΔG is the dimensionless free energy. The free energy, ΔG, has a quadratic dependence on the surface charge density of the fiber, Q_f, and the particle, Q_s:

$$\Delta G = A_1 Q_s Q_f + A_2 Q_s^2 + A_3 Q_f^2, \quad (6)$$

where values of the parameters A_1, A_2, and A_3 are given in Johnson and Deen (21) as a function of fiber and particle diameter, Debye length, and distance between particle and fiber. We calculated the individual contributions of each fiber based on Eqs 5. and 6 and the total electrostatic energy was determined as

$$E_{tot} = \sum_i E_i. \quad (7)$$

To calculate the above sum, we took into account not only the fibers residing in the cell of the particle but also the fibers in the neighboring unit cells.

Even though our methodology for the incorporation of both hydrodynamic and electrostatic interactions can be used for fiber networks of any geometry and orientation, the lack of a suitable correlation for calculating energies in a fiber network restricted our model domain to that of a square periodic array. Furthermore, because Eq. 6 was derived and tested only for repulsive interactions (21) (31), we considered only the case where the fibers and the particles have charges of same sign. Finally, we were careful to restrict the parameters of our simulations within the limits of surface charge densities, fiber and particle diameter, and Debye length for which the correlation of Johnson and Deen (21) was derived.

The charged components of the extracellular matrix that hinder diffusion of nanoparticles include collagen fibers and the associated glycosaminoglycan (GAG) chains. The collagen fibers at neutral pH have a slightly positive charge with a ζ-potential ~4mV (32), which corresponds to a surface charge density of 0.002 C/m^2. The diameter of the collagen fiber was taken to be 60 nm (33). On the other hand, GAG chains have a very small diameter (in the range of 2 nm) and a highly negative charge with surface charge density -0.10 C/m^2 (31). Molecules and nanoparticles can vary considerably both in size and charge. Here, we considered particles in the size range of 1–10 nm and surface charge density $|Q_s|$ ranging from 0.0 to 0.10 C/m^2, which is within the range reported in (34) for gold nanoparticles and consistent with values used previously in similar studies (21,31). Except where noted otherwise, the physiological ionic strength of 0.15M was used.

Preparation of extracellular matrix-mimetic gels

Collagen hydrogels were polymerized by mixing the following components in order on ice: 97.7μL of 9.37mg/mL acid-soluble rat tail tendon collagen (BD Biosciences, San Jose, CA) and 2.3μL of sodium hydroxide (1N). Optical imaging of these gels with second harmonic generation (SHG) multiphoton microscopy (MPM) revealed that the collagen fibers were isotropic and three-dimensional in nature (Fig. S1 in the Supporting Material), whereas their organization was poor with dense arrays of short fibers. After vortexing, quantum dot samples were introduced and the mixture was immediately pipetted onto coverslips that were subsequently sealed in petri dishes with a drop of water at the edge (Fisher Scientific, Pittsburgh, PA). The samples were then incubated for 1h at 37°C. The final concentration of collagen was 9.15mg/mL, which closely matched the reported values for extracellular matrix concentrations in solid tumors (6,35).

After the incubation period, coverslips containing the gel samples were sealed in glass microwell slides (VWR International, West Chester, PA) and MPM or multiphoton fluorescence correlation spectroscopy (MP-FCS) measurements were performed at room temperature. For each quantum dot type, three gel samples were used to determine the diffusion coefficient. Collagen structure and organization was visualized using second harmonic generation (SHG) imaging with MPM (36). MP-FCS measurements were performed with laser powers of 0.4–0.7 mW to avoid excitation saturation.

Quantum dot preparation

We prepared quantum dots of two different charges by modifying the surface of CdSe/CdZnS quantum dots with two derivatives of dihydrolipoic acid (DHLA), i.e., DHLA-polyethyleneglycol (DHLA-PEG) and amino-functionalized DHLA-PEG (DHLA-PEG-NH_2) using a previously reported method (37). Characterizations of the hydrodynamic radius and ζ-potential (the electrostatic potential generated by the accumulation of ions at their surface) for each quantum dot sample were performed using a dynamic light scattering (DynaPro Dynamic Light Scatterer) and ζ-potential measurement system (Brookhaven ZetaPALS, Holtsville, NY), respectively. The diffusivity in the solution was measured with a MP-FCS. The radius, ζ-potential, and diffusivity in solution of the two types of nanoparticles are given in Fig. 3 *a*.

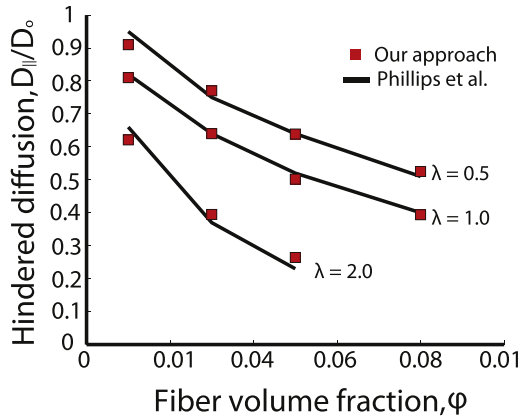

FIGURE 2 Our approach compared to the results of Philips et al. (12,22) for spatially periodic arrays of fibers. λ is the ratio of particle diameter to fiber diameter.

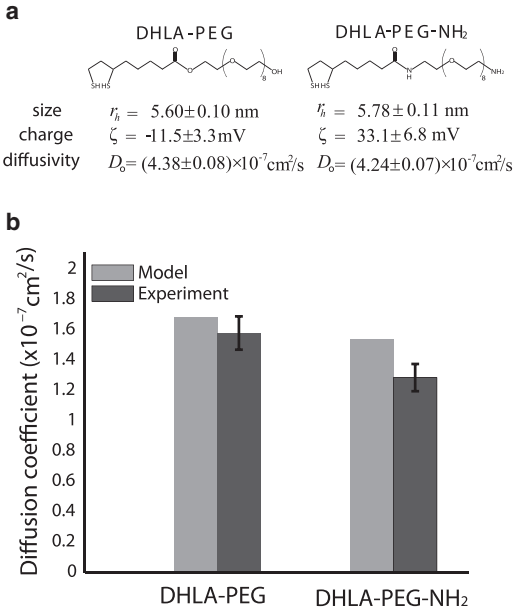

FIGURE 3 (*a*) Characteristic properties, radius, charge, diffusivity in solution, of the two types of nanoparticles. (*b*) Experimentally measured diffusivities and model predictions of the nanoparticles in collagen gels.

RESULTS

Model validation

We first validated the model predictions with the mathematical approach of Phillips et al. (12,22), who calculated the diffusion of particles in a spatially periodic square array of fibers, taking into account only steric and hydrodynamic interactions. They used the same Stokesian dynamics method to account for hydrodynamic hindrance, but instead of employing a random walk to calculate the overall diffusion coefficient, they used the generalized Taylor dispersion theory. Fig. 2 shows that our simulations agree well with the results of Phillips et al.

We also tested our model predictions with diffusion measurements of quantum dot nanoparticles in collagen gels that mimic the extracellular matrix of tumors. We used two types of quantum dots with similar size but different charge. The DHLA-PEG were considered to be near neutral, whereas the DHLA-PEG-NH_2 had a highly positive charge. To apply the model to collagen gels we had to account for the increase in the viscosity of the aqueous phase due to unassembled collagen that does not form fibers but stays in the solution as collagen oligomers. The viscosity can be calculated by the volume fraction and the aspect ratio of the unpolymerized collagen (Eq. 6.4 in Clayes and Brady (38)). We measured the volume fraction by performing spectrophotometric analysis of the supernatant of the gel after centrifugation and found that 25% of the collagen stays in the solution. However, there is no direct method to measure the aspect ratio, which makes it difficult to calculate the exact value of the viscosity and subsequently the diffusion coefficient. Here, we are interested in using the model to predict the relative diffusivity between the two types of nanoparticles. Based on the fact that collagen forms elongated rods of high aspect ratio, and with the understanding that the viscosity is inversely proportional to the diffusivity, we used an aspect ratio of 60 (the highest aspect ratio reported in (38)), which increases the viscosity of water by a factor of 2.7. The surface charge density of the particles was calculated by the ζ-potential (Fig. 3 *a*), using the Gouy-Chapman electric double layer theory. The diameter of the collagen fiber was taken to be 60 nm (33) and the ζ-potential 4 mV (32). The fiber volume fraction was calculated from the concentration used to make the gels and the collagen's effective specific volume (1.89 ml/g) (6). Fig. 3 *b* shows that the diffusivity of the positively charged quantum dots is lower than the diffusivity of the near neutral particles both in the experiment and the model. Additionally, Fig. S2 shows that the near neutral particles distribute more homogeneously compared to the positively charged particles.

Electrostatic repulsion is important when fiber diameters are comparable to the Debye length

In Figs. 4 and 5, we assumed a uniform negative fiber surface charge density and we kept the fiber volume fraction and the ratio of the particle diameter to the fiber diameter, λ, constant. We used two values for the ionic strength of the interstitial fluid: the physiological ionic strength value of 0.15M as well as a much lower ionic strength of 0.02M for comparison. Fig. 4, *a* and *b*, presents the overall diffusion coefficient transverse to the preferred fiber direction for ionic strength 0.15M, and Fig. 5, *a* and *b* presents the results for 0.02M. Fig. S3 and Fig. S4 show the diffusivity parallel to the preferred fiber direction. The range of electrostatic interactions is governed by the Debye length, k_d^{-1}. The Debye length, which is inversely proportional to the square root of the ionic strength, was 0.79 nm at 0.15M and

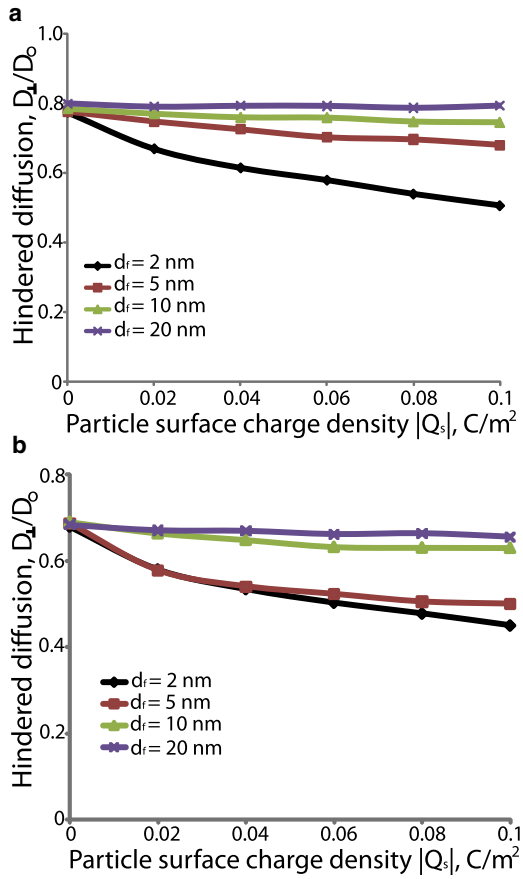

FIGURE 4 Effect of electrostatic repulsion on the hindered diffusion of nanoparticles. The fiber surface charge density was taken to be −0.05 C/m^2, the ionic strength of the solution was set to 0.15M and λ was 0.5. The fiber volume fractions were 0.03 (*a*) and 0.06 (*b*). Hindered diffusion is the ratio of the overall diffusion coefficient in the fibrous medium transverse to the fiber direction, $D_\perp$, over the diffusion coefficient in solution, D_o.

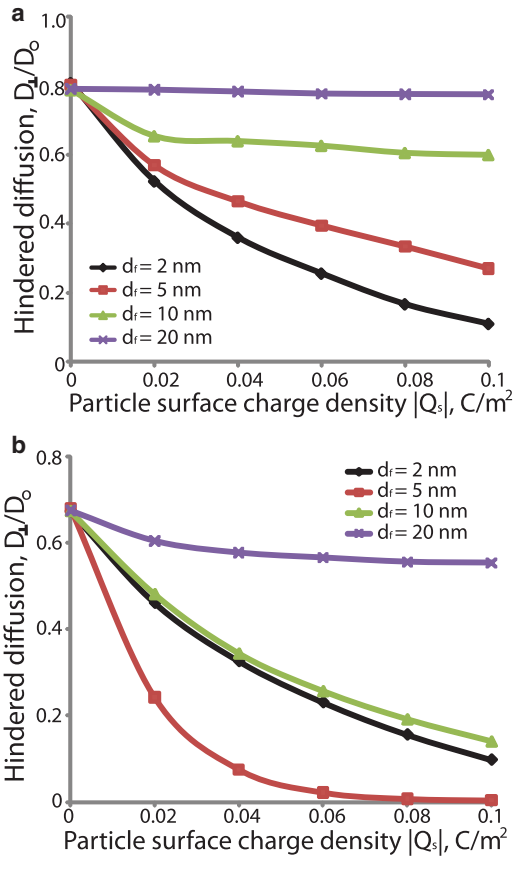

FIGURE 5 Effect of electrostatic repulsion on the hindered diffusion of nanoparticles. The fiber surface charge density was taken to be −0.05 C/m^2, the ionic strength of the solution was set to 0.02M and λ was 0.5. The fiber volume fractions were 0.03 (*a*) and 0.06 (*b*). Hindered diffusion is the ratio of the overall diffusion coefficient in the fibrous medium transverse to the fiber direction, $D_\perp$, over the diffusion coefficient in solution, D_o.

2.16 nm at 0.02M. From both Figs. 4 and 5, we conclude that electrostatic repulsion hinders diffusion of negatively charged particles for small fibers but has little effect for large fibers. When the fiber diameter, d_f, is comparable to the Debye length, the range of electrostatic forces is comparable to the size of the fibers. However, when the fiber size is much larger than the Debye length, the range of electrostatic forces forms a very small envelope that surrounds the fiber (Fig. 6). Therefore, repulsive electrostatic interactions are significant for diffusion of particles around fibers whose size is comparable to the Debye length.

Fiber volume fraction increases the effect of electrostatic interactions

Electrostatic interactions also depend on fiber volume fraction. We repeated the simulations in Figs. 4 and 5 for two fiber volume fractions, 0.03 and 0.06. At a 0.03 volume fraction, electrostatic interactions are not as strong and the diffusivity increases as the fiber diameter increases (Figs. 4 *a* and 5 *a*). At a 0.06 volume fraction, however, the fibers are packed closer together and electrostatic forces become more important (Fig. 6). For fibers with diameter of 5 nm, the diffusivity is similar or lower than the diffusivity for 2 nm fibers, whereas for larger fibers (>5 nm) the diffusivity increases again (Figs. 4 *b* and 5 *b*).

Ionic strength significantly affects the diffusivity of charged particles

As the ionic strength increases, the Debye length decreases and the effect of electrostatic interactions diminishes. A comparison of Figs. 4 and 5 shows the dramatic decrease in the mobility of the particle caused by changing the ionic strength from 0.15 to 0.02M. Furthermore, Fig. 7 and Fig. S5 show the hindered diffusion of a particle as a function of its surface charge density for four different values of the ionic strength, 0.02M, 0.06M, 0.1M, and 0.15M. Again, we see that increasing the ionic strength increases the diffusivity of the particle.

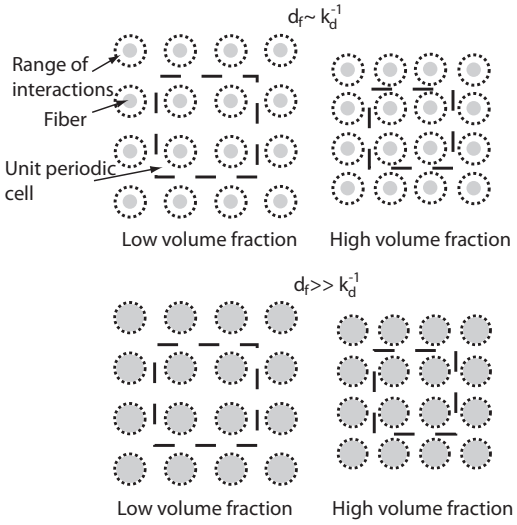

FIGURE 6 Spatially-periodic arrangement of fibers for low and high fiber volume fractions. As the fiber volume fraction increases the fibers are packed closer to each other. Therefore, the range of electrostatic interactions for fibers with diameter, d_f, comparable to the Debye length, k_d^{-1} increases.

Particle size affects both hydrodynamic and electrostatic interactions

Fig. 8 shows the hindered diffusion transverse to the preferred fiber direction as a function of the particle surface charge density and when the ratio of particle diameter to fiber diameter, λ, is 0.5, 1.0, 2.0, and 3.0. For uncharged particles the diffusion coefficient decreases as a result of steric and hydrodynamic interactions. For charged particles, electrostatic forces cause an almost uniform decrease in the diffusivity of the particles. Fig. S6 presents the results for diffusion parallel to the preferred fiber direction. Interestingly, we see that diffusivity in the preferred fiber direction

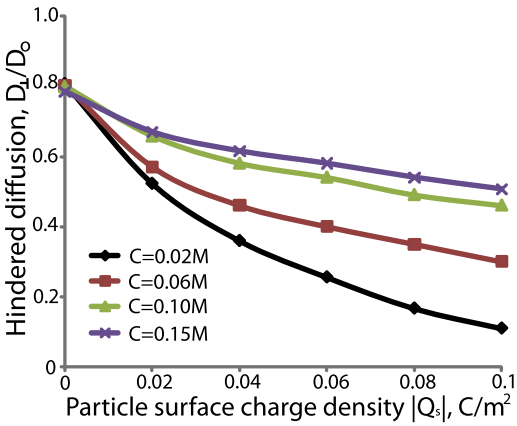

FIGURE 7 Effect of ionic strength on the hindered diffusion of nanoparticles. The fiber volume fraction, φ, was set to 0.03, the fiber diameter, d_f, and surface charge density, Q_f, were 2 nm, and −0.05 C/m^2, and the ratio of particle size to fiber size, λ, was 0.5.

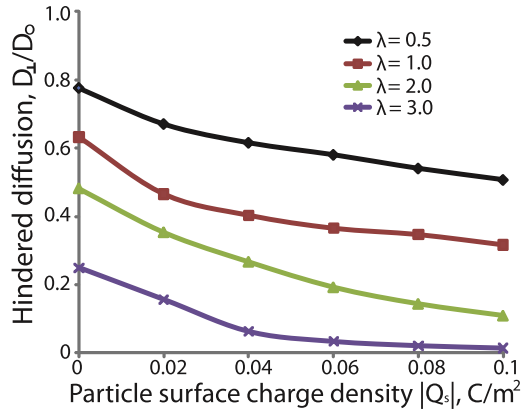

FIGURE 8 Effect of particle size on the hindered diffusion of nanoparticles. The fiber volume fraction, φ, was set to 0.03, the fiber diameter, d_f, and surface charge density, Q_f, were 2 nm, and −0.1 C/m^2, and the ionic strength was 0.15M.

is independent of the surface charge density of particles with $\lambda = 2.0$ and $\lambda = 3.0$.

DISCUSSION

According to our results, the effect of repulsive electrostatic interactions on the diffusion of nanoparticles is significant only when the fiber size is comparable to the Debye length (Figs. 4 and 5). For glycosaminoglycan chains, the size is a few nanometers and the effect is potentially important. However, for larger fibers such as collagen, the effect of repulsive forces becomes less significant. Also, comparison of the diffusion coefficients parallel and transverse to the preferred fiber direction shows that the mobility of charged particles is affected more in the transverse direction. Experimental studies (17,18) have shown decreases in the diffusion coefficient of positively and negatively charged nanoparticles (up to three orders of magnitude) in reconstituted ECM hydrogels due to electrostatic attraction and binding. Here, we propose that under certain conditions — e.g., small fibers and low ionic strength — electrostatic repulsion might have similar effects. The model predictions of the overall diffusion coefficient and its directional components (Eq. 1) can also be used in Fick's law to calculate the average or the directional diffusive flux of particles in fibrous media.

The model is limited in that the correlation (Eq. 6) used to calculate electrostatic energies has been validated only for a single fiber (21) or a spatially periodic array of fibers (31). This correlation provides an accurate way to calculate electrostatic energies without significant computational cost. Once a similar expression is available for random fiber distributions, our mathematical framework can be easily extended to incorporate fiber networks. It has been shown (39,40), however, that the overall diffusion coefficient is affected only by the fiber volume fraction and not the fiber

distribution. Therefore, we expect our predictions to be meaningful for fiber networks. Another limitation is that Eq. 6 was derived for repulsive interactions between particles and fibers and does not consider attractive forces. Thus, our simulations were restricted to particles with the same charge as the fibers. In addition, Eq. 6 was developed based on the linearization of the Poisson-Boltzmann equation, which is valid when the surface potentials are less than the thermal potential (kT/e). In our analysis, this limitation was not always met. For repulsive interactions, however, the errors in the Boltzmann factor $\exp(-E/kT)$ are likely to be minor because $E > 0$ and $\exp(-E/kT)$ are already small. Therefore, linearization of the Poisson-Boltzmann equation should not overestimate the electrostatic energy significantly.

To our knowledge, this is the first model to incorporate both hydrodynamic and electrostatic interactions in a random walk approach for the study of diffusion in fibrous media. The Stokesian dynamics method is computationally intensive and the use of parallel processing was required to obtain solutions in acceptable times. When the particle size is very small compared to the fiber diameter, hydrodynamic interactions are not important and the Stokesian dynamics method could be excluded from the simulation (13,22). When the particle size is comparable or even larger than the fiber diameter, hydrodynamic hindrance slows down the mobility of the particle more than twofold and incorporation of hydrodynamic interactions becomes necessary. Additionally, we found that when we excluded Stokesian dynamics, we had to track the displacement of more than 200,000 random walkers to get a stable solution. At the same time, incorporation of Stokesian dynamics restricted the mobility of the particles and decreased the total number of random walkers that we used to 1000.

Nanoparticles have been developed as a promising new generation of contrast agents and targeted delivery vehicles for the diagnosis and treatment of solid tumors (41–43). Due to the importance of nanotechnology in the study and treatment of cancer, we sought to understand how particle surface charge affects transport in the ECM. It is widely accepted that cationic particles selectively target tumor vessels (3,44) and they are preferred for that reason. Here, we showed that neutral particles might diffuse faster than cationic. We also showed that for large fibers, electrostatic repulsion might not be significant and, thus, the diffusivity of particles with charge of same sign as the fibers will be the same as the diffusivity of neutral particles. The tumor microenvironment consists of fibers whose diameter ranges from a few nanometers (hyaluronic acid, collagen oligomers) up to a few micrometers (collagen fibers) and their charge can be either positive (collagen) or negative (hyaluronic acid). Therefore, neutral nanoparticles should diffuse faster than cationic. From the above analysis, we conclude that the optimal nanoparticle for delivery to tumor tissue should be initially cationic to selectively target tumor vessels, but change charge to neutral after entering the ECM.

SUPPORTING MATERIAL

Six figures are available at http://www.biophysj.org/biophysj/supplemental/S0006-3495(10)00727-7.

We thank Professors William M. Deen (Massachusetts Institute of Technology) and Ronald J. Phillips (University of California, Davis) for useful discussions.

This work was supported by the National Institutes of Health (5PO1CA080124 and RO1CA126642). T.S. was supported by a postdoctoral research fellowship from the Susan G. Komen Breast Cancer Foundation (KG091281).

REFERENCES

1. Jain, R. K. 1987. Transport of molecules in the tumor interstitium: a review. *Cancer Res.* 47:3039–3051.
2. Choi, H. S., W. Liu, …, J. V. Frangioni. 2007. Renal clearance of quantum dots. *Nat. Biotechnol.* 25:1165–1170.
3. Campbell, R. B., D. Fukumura, …, L. L. Munn. 2002. Cationic charge determines the distribution of liposomes between the vascular and extravascular compartments of tumors. *Cancer Res.* 62:6831–6836.
4. Pluen, A., P. A. Netti, …, D. A. Berk. 1999. Diffusion of macromolecules in agarose gels: comparison of linear and globular configurations. *Biophys. J.* 77:542–552.
5. Pluen, A., Y. Boucher, …, R. K. Jain. 2001. Role of tumor-host interactions in interstitial diffusion of macromolecules: cranial vs. subcutaneous tumors. *Proc. Natl. Acad. Sci. USA.* 98:4628–4633.
6. Ramanujan, S., A. Pluen, …, R. K. Jain. 2002. Diffusion and convection in collagen gels: implications for transport in the tumor interstitium. *Biophys. J.* 83:1650–1660.
7. Johnson, E. M., D. A. Berk, …, W. M. Deen. 1996. Hindered diffusion in agarose gels: test of effective medium model. *Biophys. J.* 70: 1017–1023.
8. Kosto, K. B., and W. M. Deen. 2004. Diffusivities of macromolecules in composite hydrogels. *AIChE J.* 50:2648–2658.
9. Berk, D. A., F. Yuan, …, R. K. Jain. 1993. Fluorescence photobleaching with spatial Fourier analysis: measurement of diffusion in light-scattering media. *Biophys. J.* 65:2428–2436.
10. Ogston, A. G., B. N. Preston, and J. D. Wells. 1973. On the transport of compact particles through solutions of chain-polymers. *Proc. R. Soc. Lond. A Math. Phys. Sci.* 333:297–316.
11. Johansson, L., and J. E. Lofroth. 1993. Diffusion and interaction in gels and solutions. 4. Hard sphere Brownian dynamics simulations. *J. Chem. Phys.* 98:7471–7479.
12. Phillips, R. J., W. M. Deen, and J. F. Brady. 1989. Hindered transport of spherical macro-molecules in fibrous membranes and gels. *AIChE J.* 35:1761–1769.
13. Clague, D. S., and R. J. Phillips. 1996. Hindered diffusion of spherical macromolecules through dilute fibrous media. *Phys. Fluids.* 8: 1720–1731.
14. Jin, S., Z. Zador, and A. S. Verkman. 2008. Random-walk model of diffusion in three dimensions in brain extracellular space: comparison with microfiberoptic photobleaching measurements. *Biophys. J.* 95:1785–1794.
15. Nandigam, R. K., and D. M. Kroll. 2007. Three-dimensional modeling of the brain's ECS by minimum configurational energy packing of fluid vesicles. *Biophys. J.* 92:3368–3378.

16. Hrabe, J., S. Hrabetová, and K. Segeth. 2004. A model of effective diffusion and tortuosity in the extracellular space of the brain. *Biophys. J.* 87:1606–1617.

17. Lieleg, O., R. M. Baumgärtel, and A. R. Bausch. 2009. Selective filtering of particles by the extracellular matrix: an electrostatic bandpass. *Biophys. J.* 97:1569–1577.

18. Thorne, R. G., A. Lakkaraju, …, C. Nicholson. 2008. In vivo diffusion of lactoferrin in brain extracellular space is regulated by interactions with heparan sulfate. *Proc. Natl. Acad. Sci. USA.* 105:8416–8421.

19. Dowd, C. J., C. L. Cooney, and M. A. Nugent. 1999. Heparan sulfate mediates bFGF transport through basement membrane by diffusion with rapid reversible binding. *J. Biol. Chem.* 274:5236–5244.

20. Magzoub, M., S. Jin, and A. S. Verkman. 2008. Enhanced macromolecule diffusion deep in tumors after enzymatic digestion of extracellular matrix collagen and its associated proteoglycan decorin. *FASEB J.* 22:276–284.

21. Johnson, E. M., and W. M. Deen. 1996. Electrostatic effects on the equilibrium partitioning of spherical colloids in random fibrous media. *J. Colloid Interface Sci.* 178:749–756.

22. Phillips, R. J., W. M. Deen, and J. F. Brady. 1990. Hindered transport in fibrous membranes and gels: Effect of solute size and fiber configuration. *J. Colloid Interface Sci.* 139:363–373.

23. Beenakker, C. W. J. 1986. Ewald sum of the Rotne-Pranger tensor. *J. Chem. Phys.* 85:1581–1582.

24. Kim, S., and R. T. Mifflin. 1985. The resistance and mobility functions of two equal spheres in low-Reynolds-number flow. *Phys. Fluid.* 28:2033–2045.

25. Jeffrey, D. J., and Y. Onishi. 1984. Calculation of the resistance and mobility functions for two unequal rigid spheres in low-Reynolds-number flow. *J. Fluid Mech.* 139:261–290.

26. Phillips, R. J., J. F. Brady, and G. Bossis. 1988. Hydrodynamic transport properties of hard-sphere dispersions: I. Suspensions of freely mobile particles. *Phys. Fluids.* 21:3462–3472.

27. Phillips, R. J., J. F. Brady, and G. Bossis. 1988. Hydrodynamic transport properties of hard-sphere dispersions: II Porous Media. *Phys. Fluids.* 31:3473–3479.

28. Brady, J. F., R. J. Phillips, …, G. Bossis. 1988. Dynamic simulation of hydrodynamically interacting suspensions. *J. Fluid Mech.* 195: 257–280.

29. Phillips, R. J. 1995. Calculation of multisphere linearized Poisson-Boltzmann Interactions near cylindrical fibers and planar surfaces. *J. Colloid Interface Sci.* 175:386–399.

30. Mark, L. A., J. L. Kaplan, and J. C. Williams, Jr. 2000. Exact solution to the electrostatic interaction between an ion-penetrable sphere and an ion-penetrable rod. *J. Colloid Interface Sci.* 229:102–106.

31. Bhalla, G., and W. M. Deen. 2009. Effects of charge on osmotic reflection coefficients of macromolecules in fibrous membranes. *Biophys. J.* 97:1595–1605.

32. Li, Y., A. Asadi, …, E. P. Douglas. 2009. pH effects on collagen fibrillogenesis in vitro: Electrostatic interactions and phosphate binding. *Mater. Sci. Eng. C.* 29:1643–1649.

33. Sander, E., T. Stylianopoulos, …, V. Barocas. 2009. Image-based biomechanics of collagen-based tissue equivalents. *IEEE Eng. Med. Biol. Mag.* 28:10–18.

34. Park, S., and K. Hamad-Schifferli. 2008. Evaluation of hydrodynamic size and zeta-potential of surface-modified Au nanoparticle-DNA conjugates via Ferguson Analysis. *J. Phys. Chem.* 112:7611–7676.

35. Netti, P. A., D. A. Berk, …, R. K. Jain. 2000. Role of extracellular matrix assembly in interstitial transport in solid tumors. *Cancer Res.* 60:2497–2503.

36. Brown, E., T. McKee, …, R. K. Jain. 2003. Dynamic imaging of collagen and its modulation in tumors in vivo using second-harmonic generation. *Nat. Med.* 9:796–800.

37. Liu, W., M. Howarth, …, M. G. Bawendi. 2008. Compact biocompatible quantum dots functionalized for cellular imaging. *J. Am. Chem. Soc.* 130:1274–1284.

38. Clayes, I. L., and J. F. Brady. 1993. Suspensions of prolate spheroids in Stokes flow. part 2. Statistically homogeneous dispersions. *J. Fluid Mech.* 251:443–477.

39. Erikson, A., H. N. Andersen, …, Cde. L. Davies. 2008. Physical and chemical modifications of collagen gels: impact on diffusion. *Biopolymers.* 89:135–143.

40. Leddy, H. A., M. A. Haider, and F. Guilak. 2006. Diffusional anisotropy in collagenous tissues: fluorescence imaging of continuous point photobleaching. *Biophys. J.* 91:311–316.

41. Stroh, M., J. P. Zimmer, …, R. K. Jain. 2005. Quantum dots spectrally distinguish multiple species within the tumor milieu in vivo. *Nat. Med.* 11:678–682.

42. Ballou, B., B. C. Lagerholm, …, A. S. Waggoner. 2004. Noninvasive imaging of quantum dots in mice. *Bioconjug. Chem.* 15:79–86.

43. Wu, X., H. Liu, …, M. P. Bruchez. 2003. Immunofluorescent labeling of cancer marker Her2 and other cellular targets with semiconductor quantum dots. *Nat. Biotechnol.* 21:41–46.

44. Schmitt-Sody, M., S. Strieth, …, M. Dellian. 2003. Neovascular targeting therapy: paclitaxel encapsulated in cationic liposomes improves antitumoral efficacy. *Clin. Cancer Res.* 9:2335–2341.